Generalized super-resolution 4D Flow MRI – using ensemble learning to extend across the cardiovascular system

Leon Ericsson, Adam Hjalmarsson, Muhammad Usman Akbar, Edward Ferdian, Mia Bonini, Brandon Hardy, Jonas Schollenberger, Maria Aristova, Patrick Winter, Nicholas Burris, Alexander Fyrdahl, Andreas Sigfridsson, Susanne Schnell, C. Alberto Figueroa, David Nordsletten, Alistair A. Young, David Marlevi

SUPPLEMENTARY MATERIAL

THE following document provides Supplementary Material to the paper *Generalized super-resolution 4D Flow MRI – using ensemble learning to extend across the cardiovascular system* by Ericsson, Hjalmarsson et al.

SUPPLEMENTARY MATERIAL I

Complementing **Tables II-V** in the main manuscript, **Supplementary Tables I-VIII** provides a complete list of assessed p-values for inference of statistical differences in predicted velocity distribution. Note how assessments are consistently presented across all velocity components, and across all assessed cardiovascular domains, respectively.

SUPPLEMENTARY MATERIAL II

A. Feature distribution across intermediate layers

To assess feature distribution across different layers, features were extracted from various datasets for training (one cardiac, one aortic, and one cerebrovascular) and testing (one cardiac, one aortic, and one cerebrovascular). 1000 patches of size 24x24x24 were randomly extracted from the low-resolution (LR) data along with their corresponding 48x48x8 high-resolution (HR) patches, for each model respectively. These LR patches were then used as input to the network, with features extracted at several layers: two prior to the core upsampling layer (*ResBlock3-pre* and *ResBlock6-pre*), and two after the core upsampling layer (*ResBlock2-post* and *ResBlock4-post*). Note that the use of patches follows the core training and testing setup of our architecture, necessitated by the relatively small vessel coverage compared to the entire field-of-view utilized (in average, vessel coverage ranged between approx. 5 - 35\%).

From the above, each extracted feature is represented by a 64-dimensional vector. Due to the high dimensionality, and similar to the suggested reference work, we performed dimensionality reduction using Locally Linear Embedding (LLE) with parameter settings `ncomponents` = 50 and `nneighbors` = 5. These reduced features were then subsequently processed using the Manifold Discovery Analysis (MDA) method. Clusters were computed from the ground truth high-resolution patches, while predicted clusters (from the predicted super-resolution patches) were used for MDA calculations. Upon review, we observed a similar distribution of clusters between high- and super-resolution patches. However, there was a definitive spread present across all datasets, where a small proportion of patches clustered at the lower end of the manifold distance, while the majority clustered at the higher end.

Continuing into visualization, MDA results were mapped onto a two-dimensional space plotting observed data using their relative manifold distance. As presented in **Supplementary Figure 1**, for training data we observed changes in the distribution across different layers indicating a slight trend towards more compact behavior at mature layers. Whereas no clear pattern emerged across different cardiovascular compartments (aorta vs. cardiac vs. cerebrovascular) for the training data, we did notice that the shifts in distribution between aortic and cardiac cases had a higher visual agreement compared to the cerebrovascular case; a result possibly stemming from the difference in hemodynamic agreement between the different compartments. For the test data (see **Supplementary Figure 2**), similar changes were noted, however, to a less clear degree compared to the training data.

B. Feature distribution during training

Similar MDA assessment as under (A), however isolating the final residual block (*ResBlock4-post*) and assessing its distribution at sequential epochs (5, 20, 100, and 180) were also performed. For this analysis, we utilized one training and one test case only, stemming from the cerebrovascular setup.

Presented in **Supplementary Figure 3**, we observe that at the beginning of training, a fairly random data distribution is seen. However, as the numbers of epochs progress, the topology of the feature space change. These topological changes were relatively consistent throughout the progression of the epochs for both the training and test cases. This indicates that the manifold properties of the network's feature space are gradually improving over the course of training, highlighting a converging training behaviour. However, similar to (A), an absence of continuity was again observed with respect to manifold distance ordering, possibly stemming from the skewed manifold distance input and patch-nature of our networks.

Supplementary Table I: Kolmogorov-Smirnov p-values for inferred velocity distribution corresponding to manuscript **Table II**. Data given for prediction in the aortic domain, with p-values given for velocity components in (x,y,z) separately. Bold face indicating statistical significance ($p < 0.05$).

	Aorta	Cerebral	Cardiac	Combined	Bagging-2
Aorta					
Cerebral	(**2.11e-64**, 0.215, **2.06e-26**)				
Cardiac	(**4.08e-41, 5.23e-41, 2.87e-21**)	(**2.59e-63, 7.73e-37, 4.61e-17**)			
Combined	(**6.30e-05, 3.22e-06, 5.87e-10**)	(**4.58e-75, 3.30e-07, 1.55e-18**)	(**8.65e-19, 8.62e-28, 6.49e-19**)		
Bagging-2	(**7.80e-05**, 0.7819, 0.2865)	(**2.80e-78**, 0.313, **9.12e-36**)	(**5.33e-14, 5.06e-46, 4.18e-19**)	(0.95, **2.53e-07, 3.68e-09**)	
Stacking-2	(0.997, **0.029, 0.005**)	(**1.14e-74**, 0.12, **2.42e-23**)	(**3.87e-37, 5.54e-24, 7.21e-27**)	(**0.001, 0.016, 1.59e-08**)	(**5.22e-06, 0.008**, 0.313)

Supplementary Table II: Kolmogorov-Smirnov p-values for inferred velocity distribution corresponding to manuscript **Table II**. Data given for prediction in the cardiac domain, with p-values given for velocity components in (x,y,z) separately. Bold face indicating statistical significance ($p < 0.05$).

	Aorta	Cerebral	Cardiac	Combined	Bagging-2
Aorta					
Cerebral	(**3.47e-11, 6.43e-05, 1.54e-07**)				
Cardiac	(**1.23e-08, 0.016, 2.84e-06**)	(**1.76e-20, 9.24e-11, 2.43e-14**)			
Combined	(**3.48e-07, 0.016**, 0.222)	(**7.02e-25, 1.25e-07, 1.02e-07**)	(0.809, 0.435, **9.79e-09**)		
Bagging-2	(**8.92e-05, 0.006, 0.001**)	(**3.17e-24, 0.002, 1.92e-10**)	(0.781, 0.163, 0.069)	(0.489, **0.043, 0.008**)	
Stacking-2	(**0.001**, 0.176, **0.001**)	(**1.34e-15, 0.001, 1.57e-16**)	(0.083, 0.516, 0.176)	(0.177, 0.409, **3.93e-05**)	(0.222, 0.316, 0.516)

Supplementary Table III: Kolmogorov-Smirnov p-values for inferred velocity distribution corresponding to manuscript **Table II**. Data given for prediction in the cerebrovascular domain, with p-values given for velocity components in (x,y,z) separately. Bold face indicating statistical significance ($p < 0.05$).

	Aorta	Cerebral	Cardiac	Combined	Bagging-2
Aorta					
Cerebral	(**0.022, 0.066, 0.004**)				
Cardiac	(0.932, **0.001, 0.013**)	(0.209, **0.001, 2.66e-05**)			
Combined	(0.086, 0.259, **0.020**)	(0.434, 0.717, **0.025**)	(0.054, **3.70e-05, 1.36e-05**)		
Bagging-2	(0.086, 0.131, 0.31)	(0.717, 0.278, 0.487)	(0.121, **0.045, 0.001**)	(0.8748, 0.5427, 0.1942)	
Stacking-2	(0.142, 0.111, 0.166)	(0.827, **0.072, 0.072**)	(0.571, 0.131, **2.66e-05**)	(0.4095, 0.2251, 0.8748)	(0.8517, 0.4872, 0.1801)

Supplementary Table IV: Kolmogorov-Smirnov p-values for inferred velocity distribution corresponding to manuscript **Table III**. Note that for compactness, inference was only performed for the best vs. worst network with respect to relative error in each parametric evaluation (number of base learners, compartmentalized vs. non-compartmentalized, and architectural variations, respectively). Data is given for prediction in the aortic domain, with p-values given for velocity components in (x,y,z) separately. Bold face indicating statistical significance ($p < 0.05$).

Number of base learners		Compartmentalized vs. Non-compartmentalized		Architectural variation	
	Bagging-12		Bagging Comp-3		Bagging-Blocks-3
Stacking-12	(0.176, **5.08e-05**, 0.666)	Stacking-3	(**1.16e-83, 0.001, 3.75e-08**)	Stacking Blocks-3	(0.587, 0.127, **0.071**)

Supplementary Table V: Kolmogorov-Smirnov p-values for inferred velocity distribution corresponding to manuscript **Table III**. Note that for compactness, inference was only performed for the best vs. worst network with respect to relative error in each parametric evaluation (number of base learners, compartmentalized vs. non-compartmentalized, and architectural variations, respectively). Data is given for prediction in the cardiac domain, with p-values given for velocity components in (x,y,z) separately. Bold face indicating statistical significance ($p < 0.05$).

Number of base learners		Compartmentalized vs. Non-compartmentalized		Architectural variation	
	Bagging-12		Bagging Comp-3		Bagging-Blocks-3
Stacking-12	(0.604, 0.043, 0.275)	Stacking-3	(**0.012**, 0.2026, **0.007**)	Stacking Blocks-3	(0.338, 0.664, **0.003**)

Supplementary Table VI: Kolmogorov-Smirnov p-values for inferred velocity distribution corresponding to manuscript **Table III**. Note that for compactness, inference was only performed for the best vs. worst network with respect to relative error in each parametric evaluation (number of base learners, compartmentalized vs. non-compartmentalized, and architectural variations, respectively). Data is given for prediction in the cerebrovascular domain, with p-values given for velocity components in (x,y,z) separately. Bold face indicating statistical significance ($p < 0.05$).

Number of base learners		Compartmentalized vs. Non-compartmentalized		Architectural variation	
	Bagging-12		Bagging Comp-3		Bagging-Blocks-3
Stacking-12	(0.999, 0.717, 0.658)	Stacking-3	(0.658, 0.460, 0.066)	Stacking Blocks-3	(0.241, 0.460, **0.037**)

Supplementary Table VII: Kolmogorov-Smirnov p-values for inferred velocity distribution corresponding to manuscript **Table IV**. Data given for prediction in the unseen aortic dissection domain, with p-values given for velocity components in (x,y,z) separately. Bold face indicating statistical significance ($p < 0.05$).

	Aorta	Cerebral	Cardiac	Combined	Bagging-12
Aorta					
Cerebral	(**4.41e-39, 1.25e-16, 3.95e-12**)				
Cardiac	(**1.14e-60, 5.20e-08, 2.40e-26**)	(**2.35e-79, 3.77e-17, 1.26e-29**)			
Combined	(**3.24e-09, 8.78e-14, 1.28e-09**)	(**2.00e-35, 9.45e-67, 3.60e-35**)	(**7.91e-75, 3.18e-25, 6.38e-42**)		
Bagging-12	(**5.03e-27, 3.99e-06, 1.67e-29**)	(**3.68e-35, 8.61e-88, 4.43e-55**)	(**6.76e-22, 1.64e-17, 6.59e-86**)	(**5.22e-19, 5.99e-07, 2.67e-13**)	
Stacking-Blocks-3	(**1.63e-10, 7.89e-05, 8.82e-17**)	(**1.68e-39, 1.42e-93, 5.72e-33**)	(**1.49e-25, 2.62e-11, 1.79e-59**)	(**1.39e-10, 5.70e-05, 4.61e-07**)	(**1.24e-08, 6.36e-05, 1.80e-07**)

Supplementary Table VIII: Kolmogorov-Smirnov p-values for inferred velocity distribution corresponding to manuscript **Table V**, the recovery of native *in-vivo* resolution. Data given for prediction across the three different *in-vivo* settings (aorta, cardiac, and cerebral), evaluating the three select models used in the main manuscript (combined baseline, bagging-12, and stacking comp-3). p-values are given for velocity components in (x,y,z) separately. Bold face indicates statistical significance ($p < 0.05$).

	Aorta		Cardiac		Cerebral	
	Combined	Bagging-12	Combined	Bagging-12	Combined	Bagging-12
Combined						
Bagging-12	(0.511, **1.67e-05, 0.005**)		(**0.076**, 0.385, **0.012**)		(0.948, 0.746, 0.852)	
Stacking Comp-3	(**0.001**, 0.438, **0.014**)	(0.176, **0.001**, 0.969)	(0.177, 0.317, **0.023**)	(0.834, 0.965, 0.296)	(0.852, 0.515, 0.571)	(0.961, 0.827, 0.746)

Supplementary Figures 1-3 are provided on the following pages.

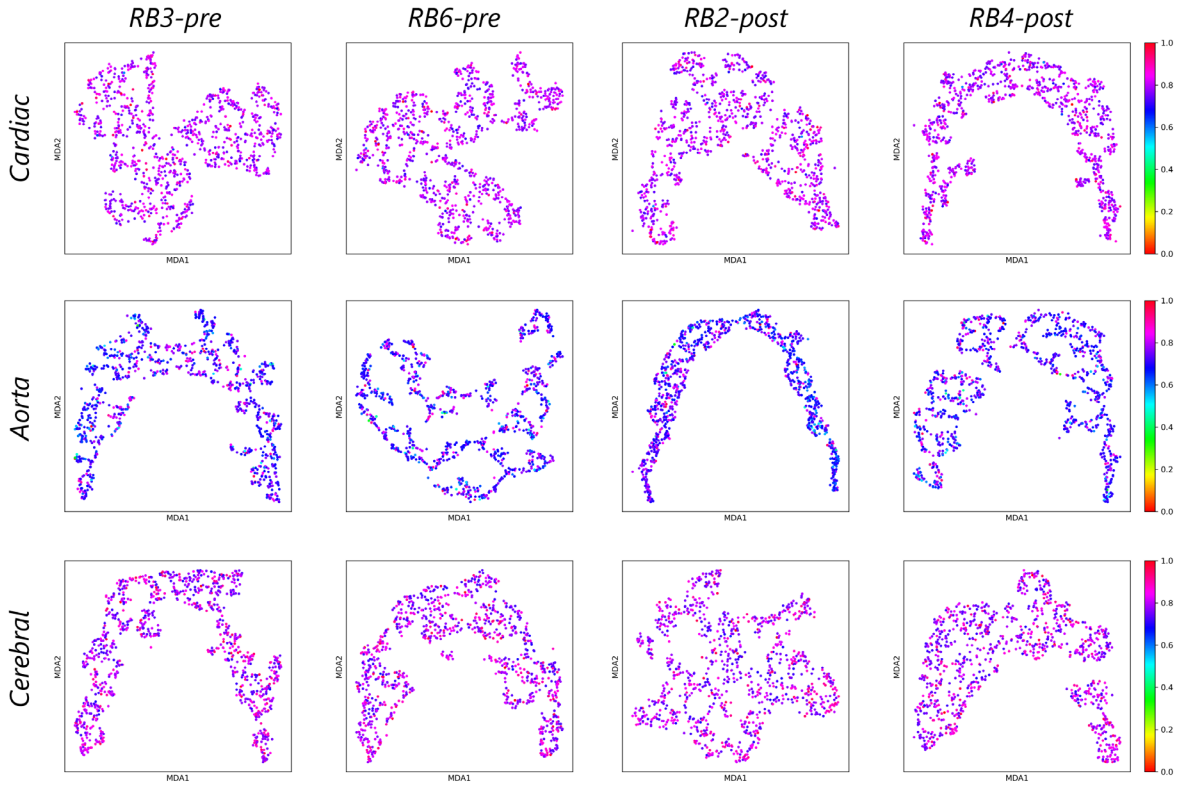

Supplementary Figure 1: MDA results for different network layers, shown for one cardiac, aortic, and cerebral training case, respectively. The color scale is given as the normalized manifold distance.

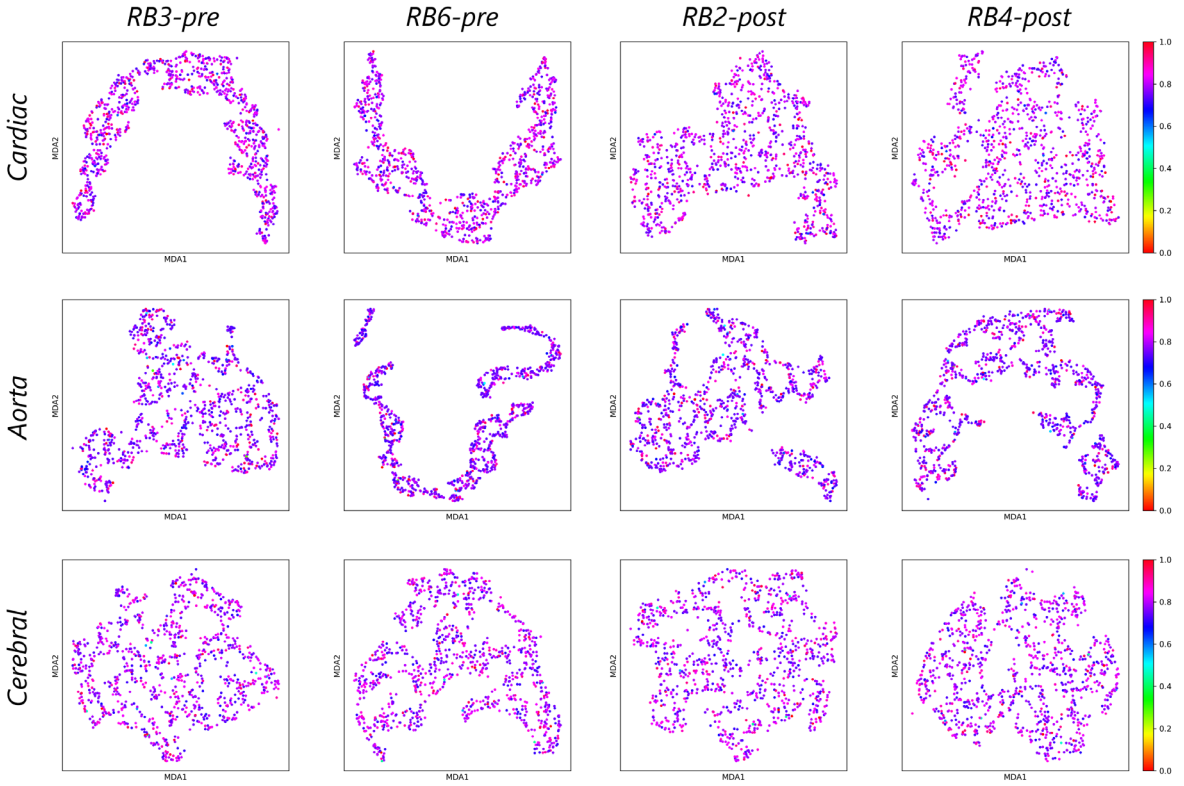

Supplementary Figure 2: MDA results for different network layers, shown for one cardiac, aortic, and cerebral test case, respectively. The color scale is given as the normalized manifold distance.

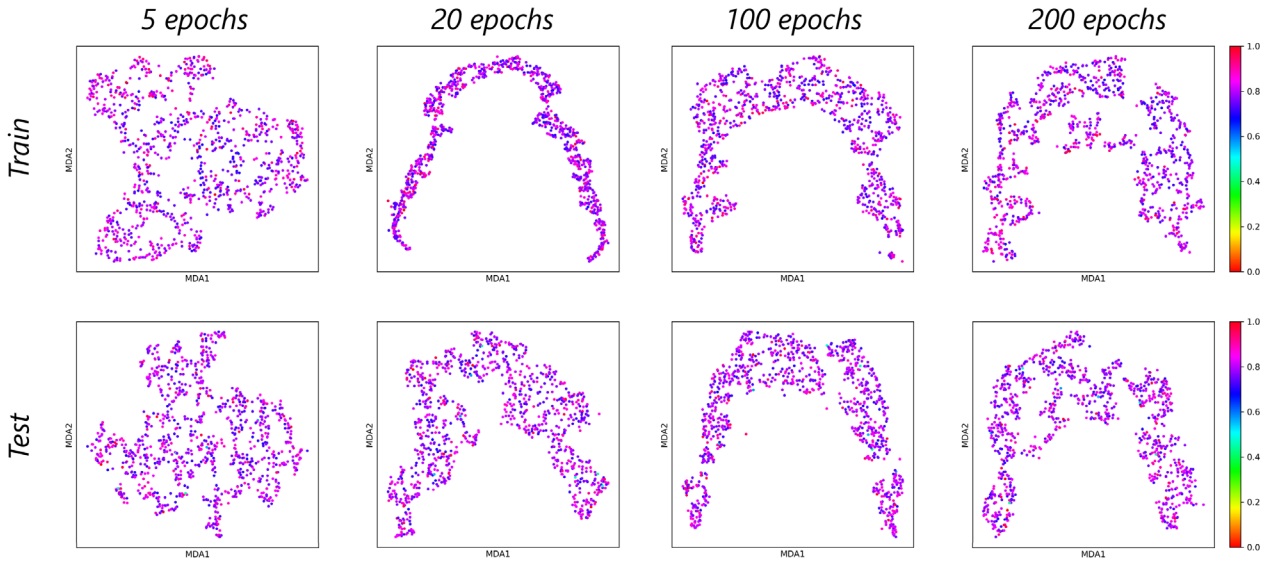

Supplementary Figure 3: MDA results for sequential epochs, shown for one training and one testing case (both sampled from the cerebral domain). The color scale is given as the normalized manifold distance.